



eXtreme Resolution (XR) mass spectrometry imaging of glycosphingolipids

As a major constituent of cellular membranes, glycosphingolipids (GSLs) play an important role in various aspects of molecular biology. Despite their importance, the analysis and interpretation of GSLs is complicated by the vast molecular heterogeneity exhibited by these molecules.

Abstract

Currently, mass spectrometry imaging is the only analytical platform capable of unraveling some of the chemical complexity of GSLs in a spatially correlated manner. Here a 15 T 2xR solariX MRMS instrument was used to increase the specificity, sensitivity and depth of GSL coverage by eXtreme Resolution (XR) MALDI Imaging. Ultimately, XR analysis (~294,000 mass resolution at 30×30 μm^2 spatial resolution) resulted in the assignment of 106 GSL species (max. error ± 1 ppm), more than double the number compared to analysis at lower mass resolution (~43,000) comparable to state-of-the-art TOF MS platforms.

Keywords:
2xR, MRMS, MALDI Imaging,
Glycosphingolipids, Imaging,
Lipidomics

Introduction

Glycosphingolipids (GSLs) are a highly complex subclass of the lipidome and are predominantly located in cell membranes. They are commonly involved in cell-cell interactions, such as recognition, adhesion and communication [1, 2]. This makes GSLs an interesting molecular class to investigate in many aspects of health and disease, such as immunity, cancer, and neurodegenerative disorders [3-5]. GSLs have two main components: the ceramide, composed of a sphingoid base and a fatty acid, as well as an oligosaccharide moiety. Despite considerable heterogeneity in the ceramide (i.e. carbon chain length, hydroxylation, saturation), the nomenclature and functional descriptions of GSLs are mainly based on its oligosaccharide

structure [1]. Given their complexity, mass spectrometry (MS) is commonly applied to identify and quantify GLSs in biological specimen. Although intact analysis of GSLs is performed [6], it is more common to dissociate the glycan and lipid moieties and analyze them separately [7, 8]. Mass spectrometry imaging is currently the only available analytical tool that is able to pinpoint GSLs to a specific location in a tissue. As such, there have been various approaches for improving the sensitivity and specificity of GSL analysis, such as chemical derivatization [9, 10], tissue treatment strategies [11, 12], and MALDI-2 ionization [4]. One underexploited strategy is the use of eXtreme Resolution (XR) mass spectrometry to improve measurement sensitivity as well as increase the number of molecular identity assignments. Magnetic resonance mass spectrometry (MRMS) is an often applied platform for XR analysis, and the recent introduction of quadrupolar (2xR) detection has shown to benefit throughput, mass resolution and sensitivity [13]. Typically coupled to low magnetic field strength magnets, here 2xR detection in a 15 T magnetic field was applied to assess whether it further enhanced mass resolution and sensitivity for the analysis of intact GSLs in healthy mouse brain tissue.

Methods

How to perform (-)MALDI Imaging of glycosphingolipids

A fresh frozen mouse brain was sectioned producing 10 μm thick tissue sections covering the transverse anatomical plane. Sections were thaw-mounted onto indium-tin-oxide-coated glass slides (Bruker Daltonics GmbH & Co. KG, Bremen, Germany) and stored at -80°C until further use. Sample preparation for glycosphingolipid analysis was based on work published by Yang *et al.* [14]. In short, slides were transferred from -80°C to room temperature using a vacuum freeze-drier. Tissues were washed using a 75 mM ammonium formate solution at pH 7 for 30 seconds, after which 1,5-diaminonaphtalene (1,5-DAN, Supelco-Merck, Amsterdam, The Netherlands) was sublimated to the glass slide using the Sublimator T1 (HTX, Chapel Hill, NC, USA). Negative ion-mode MALDI Imaging was performed on a 15 T solariX 2xR MRMS platform (Bruker Daltonics GmbH & Co. KG, Bremen, Germany) equipped with dynamically harmonized ParaCell using quadrupolar detection (2xR). The instrument was externally calibrated using red phosphorus. To further reduce the systematic mass deviation during the imaging measurements, the number of laser shots was lowered during calibration to match the red phosphorus total ion count to those achieved from tissue. The following parameters were used for all measurements with data size of 512k, 1M and 4M: Laser power 18% with minimum focus size and 10 laser shots per pixel, collision cell RF frequency of 1.4 MHz with an RF amplitude of 2 kV, TOF of 1.5 ms and a transfer frequency of 1 MHz. The ParaCell was shimmed for -3.0 V trapping. After the MALDI Imaging analysis, data was imported into SciLS™ Lab PRO (v2023b; Bruker Daltonics) for visualization. For molecular identity annotations, overall average spectra were exported as .csv files from flexImaging (v5.0; Bruker Daltonics GmbH & Co. KG, Bremen, Germany), and loaded in mMass [15]. Peak picking was performed with $\geq 0.1\%$ relative

intensity threshold. Spectra were recalibrated based on several known glycosphingolipid species, and the mMass “Compounds Search” tool was used for mass matching the peak list against the LIPIDMAPS database (subset: Sphingolipids [SP] containing 1215 entries) with a mass error tolerance of ± 1 ppm.

Table 1
Relevant method parameters for the three methods used for detection of glycosphingolipids by (-)MALDI-MRMS imaging.

	Method 1	Method 2	Method 3
<i>m/z</i> low (Da)	551.44	551.44	551.44
<i>m/z</i> high (Da)	3010.00	3010.00	3010.00
Datapoints	512k	1M	4M
Transient length (s)	0.6291	0.6291	2.5166
Detection mode	XR	2xR	2xR

Results and Discussion

To assess the effects of the 2xR detection in the m/z range required for intact GSL analysis a comparison was made in which the transient length (in ms) was kept equal (Figure 1; XR (grey): 512k, 629 ms; 2xR (red); 1M, 629 ms), which should benefit the mass resolution of the analysis. A strong increase in the number of low intensity m/z features (relative intensity <1%; $FC_{2xR/XR} = 1.56$) was observed, indicating an increased measurement sensitivity for the 2xR analysis (Figure 1A). As was expected, the measured mass resolution in the 2xR analysis approximately doubled compared to XR analysis ($FC_{2xR/XR} = 1.99$, Figure 1B). The increased number of detected features was only relevant if assigned to a molecular identity. Using 2xR detection substantially more GSL structures were assigned to m/z features ($FC_{2xR/XR} = 1.75$). For low intensity features, gained in the 2xR analysis, this was more than double (relative intensity <1%; $FC_{2xR/XR} = 2.14$, Figure 1C).

Upon a further increase of mass resolution, by extending the transient (Figure 1; 2xR (dark blue): 4M, 2.52 s), all of the previous observations were exacerbated. Compared to the 2xR-1M analysis, the 2xR-4M analysis exhibited an increase in the total number of detected m/z features ($FC_{4M/1M} = 1.41$), a tripled average peak resolution of 294,000 ($FC_{4M/1M} = 3.4$), and a 22% increase in assigned GSLs, albeit at a reduction of analysis throughput. Compared to the XR-512k analysis which had an average mass resolution of ~43,000, comparable to state-of-the-art time-of-flight MS platforms, the number of assigned GLS species was more than doubled. Clearly, the increased mass resolution benefited the analysis of complex mixtures, as it allowed

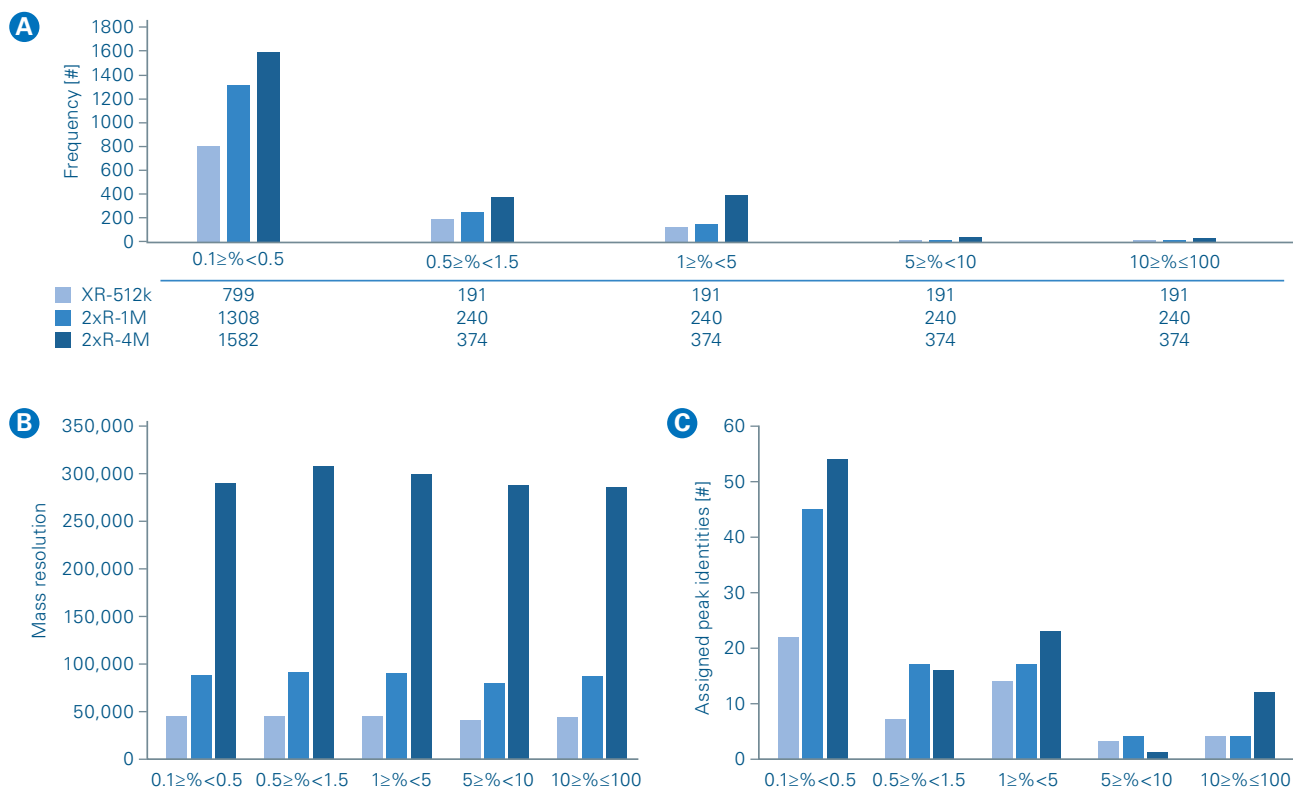


Figure 1

The effect of mass resolution on measurement sensitivity and the assignment of glycosphingolipids to (-)MALDI Imaging peaks.

(A) Results of peak picking at a $\geq 0.1\%$ relative intensity threshold following MALDI-MRMS imaging at different transient lengths. The bars represent the number of picked peaks in the various relative intensity bins. **(B)** Average mass resolution for peaks in the respective relative intensity bins. **(C)** Number of peaks assigned to a glycosphingolipid (± 1 ppm) within the respective relative intensity bins.

to resolve low intensity species from chemical background based on accurate mass and similarities between spatial distributions of chemically related species (Figure 2).

Next, the heterogeneity of the assigned GSL species on both the ceramide and the oligosaccharide level was investigated further (Figure 3). It was found that most GSLs contain either a Cer(d36:1), Cer(d38:1) or Cer(d40:1) lipid portion (Figure 3A). This was in line with a previous report extensively studying GSLs in murine tissues using microdissection and LC-MS-based approaches [16]. Another report highlighted the abundance of the different oligosaccharide moieties attached to the ceramides [17], which corroborated the finding that GD1 and GM1 glycans were the predominant species (Figure 3C). "Other negative" GSL species were additionally found which were assigned with an oligosaccharide composition but not assigned to a specific GSL subclass due to structural overlap between subclasses. Since the analysis was performed on mouse tissue, different neuraminic acid residues were to be expected. While *N*-acetylneuraminic acid (NeuAc) was predominant, various GSLs decorated with *N*-glycolylneuraminic acid (NeuGc) or mixtures of both were observed (Figure 3E). Despite the large number of peak identity assignments, due to the molecular complexity of the GSLs *in-situ* tandem-MS studies will be required to conclusively identify all species (Figure 3F). Here this was prohibited due to the complex nature of the sample and low abundance of many of the assigned GSL species.

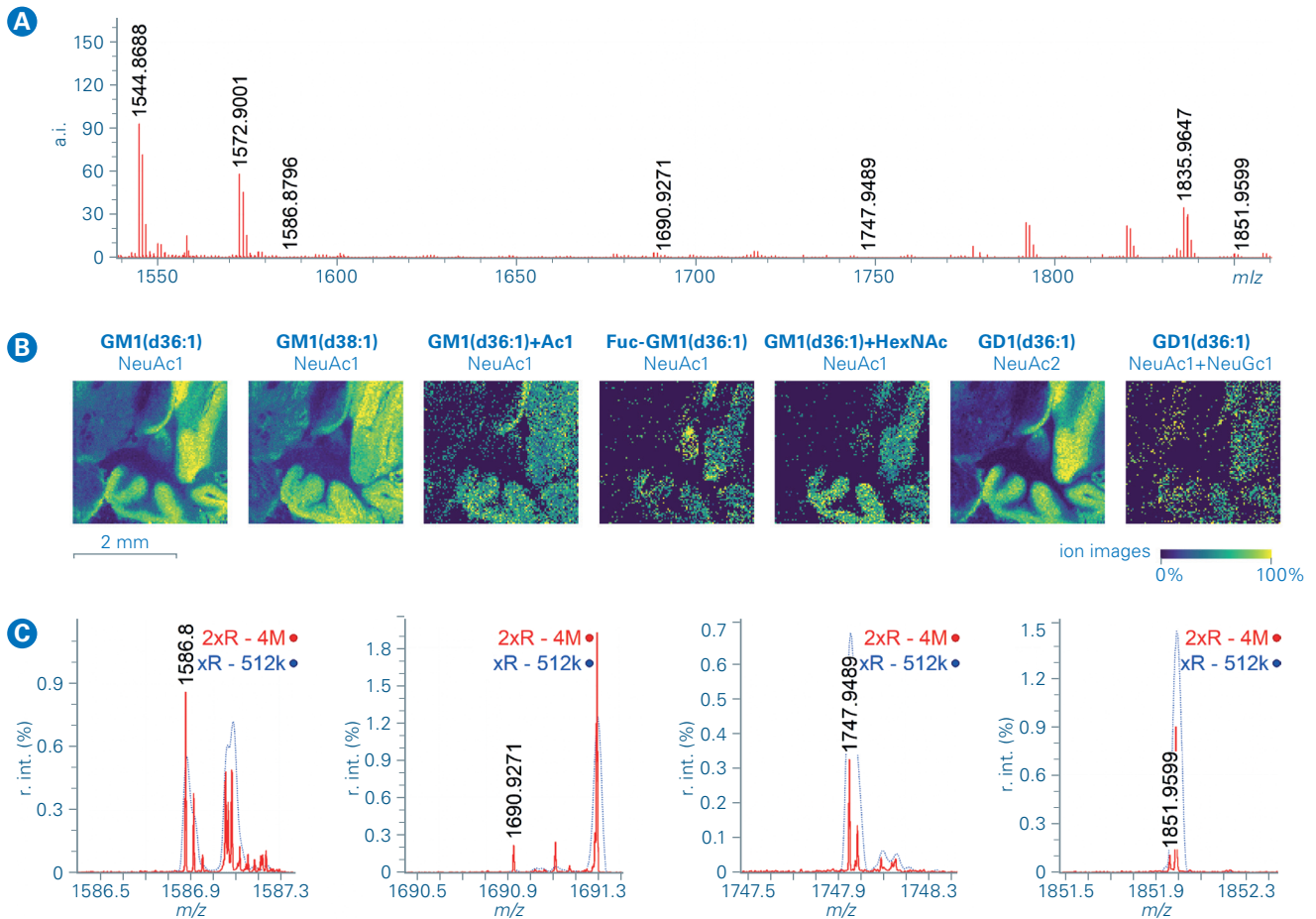


Figure 2
Glycosphingolipids in the cerebellum of the mouse brain.

(A) Overall average spectrum of a transverse section of a mouse brain. The cerebellum was analyzed at a $30 \times 30 \mu\text{m}^2$ pixel size using a 4M datapoint transient. The m/z values indicated correspond to the images and molecular annotations in (B) from left to right. (C) Zoom-ins ($\pm 0.4 m/z$) on the peaks assigned to GM1(d36:1)+Ac1, Fuc-GM1(d36:1), GM1(d36:1)+HexNAc and GD1(d36:1). The blue spectrum in (C) is the average spectrum of an adjacent section analyzed using a 512k datapoint transient in XR-mode.

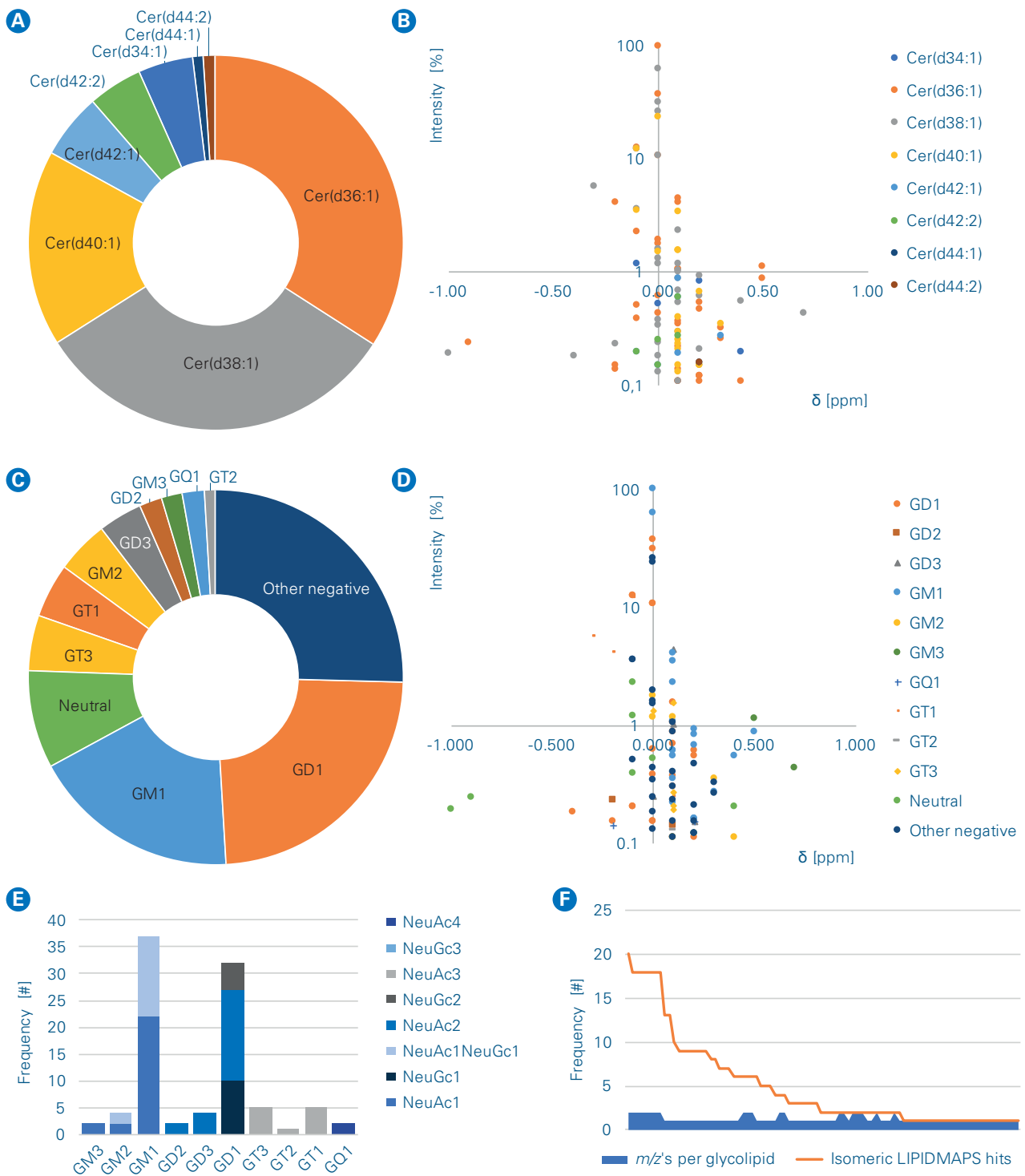


Figure 3

Glycosphingolipid assignments.

(A) The various ceramides found in the assigned glycosphingolipid species and in **(B)** their relative intensities and relative mass errors. **(C)** The various oligosaccharides found in the assigned glycosphingolipid species and in **(D)** their relative intensities and relative mass errors. **(E)** Sialylation variants of the assigned glycosphingolipids. **(F)** Number of m/z values per assigned glycosphingolipid (blue) and the number of isomeric structures in the LIPIDMAPS database (orange), highlighting the complexity of glycosphingolipid analysis.

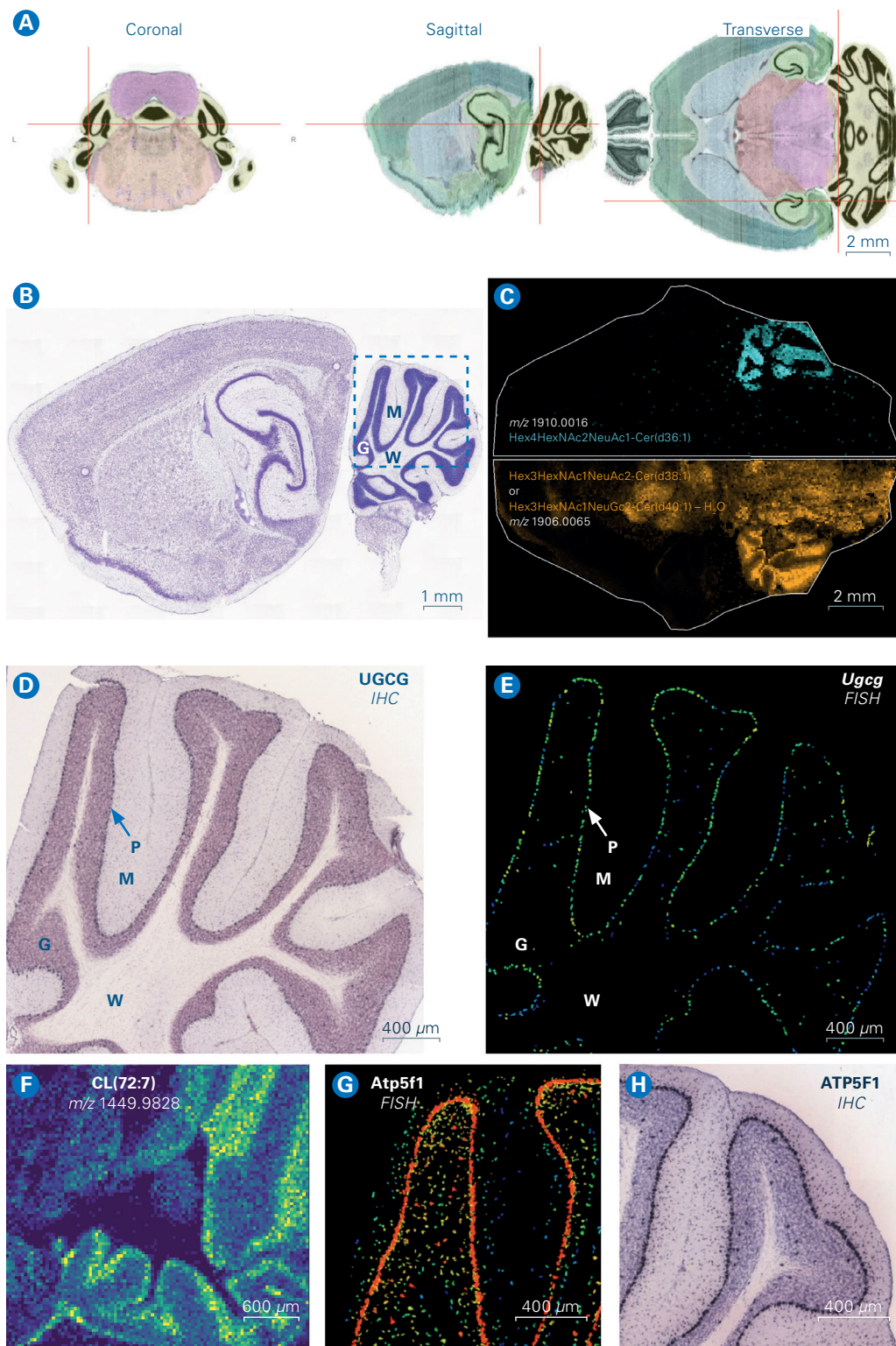


Figure 4

Brain distribution of glycosphingolipids and their associated genes.

(A) The Allen Brain Atlas (ABA) Anatomical Gene Expression Atlas (AGEA) allowed the identification of the exact brain area on which MALDI Imaging was performed. It also allows the navigation between the various anatomical planes. **(B)** Nissl-stained sagittal section taken from the ABA. **(C)** Distribution of two glycosphingolipid peaks. The extended-GD1 structure (cyan) finds itself mostly in the molecular layer (M) of the cerebellum. The GD1 structure (orange) is more widely spread but is mainly located in the granular layer (G) of the cerebellum. None of the glycosphingolipids is located in the white matter (W). The expression of UDP-glucose ceramide glucosyltransferase (UGCG) strongly correlates with the Purkinje cells (P), granular and molecular layer **(D)**, while in the cerebellum its gene (*Ugcg*) is exclusively expressed in the Purkinje cells **(E)**. Mitochondrial cardiolipin **(F)**, and the expression of mitochondrial ATP synthase F0 complex, subunit B1 gene **(G)** and protein **(H)**.

In order to validate the distributions observed for many of the assigned GSL species the Allen Brain Atlas (ABA; <https://mouse.brain-map.org/static/atlas>) was used to study the localization of UDP-glucose ceramide glycosyltransferase (protein: UGCG; gene: *Ugcg*), the enzyme facilitating the binding of the initial glucose-residue to the ceramide lipid (Figure 4). Most of the GSLs observed by MALDI Imaging were located in the molecular and granular layers, as well as in the Purkinje cells of the cerebellum (Figures 2B and 4C). It was evident from the ABA fluorescence *in-situ* hybridization (FISH) data that in the murine cerebellum the *Ugcg* gene was exclusively expressed in the Purkinje cells (Figure 4E). Based on ABA immunohistochemistry (IHC) data it was found that the UGCG enzyme itself was also present in the granular layer, and to a lesser extent in the molecular layer (Figure 4D).

Worth noting is that the current method, while targeted at GSLs, did not only result in the analysis of GSL species. Using METASPACE [18, 19], a total of 41 *m/z* features was assigned to cardiolipin species with high confidence. Upon visual inspection, the cardiolipins all appeared to colocalize with the Purkinje cells (Figure 4F). Since cardiolipins are exclusively found in the mitochondrial membranes a validation by comparing the cardiolipin distributions with the distribution of the mitochondrial ATP synthase protein was pursued (protein: ATP5F1; gene: *Atp5f1*; Figures 4G and H). Both gene expression and protein abundance strongly correlated with the Purkinje cell layer.

Conclusion

Spatial analysis by eXtreme Resolution (XR) MALDI Imaging using a 15 T 2xR MRMS instrument was performed for detection of large, complex and highly relevant lipid species, including GSLs and cardiolipins. The enhanced, and ultra-high mass resolution accessible at reasonable throughput as reflected by the longer transient length and by applying 2xR detection, showed paramount in detecting these specific lipid classes, and assigning molecular identities to recorded images. As such it provides a powerful tool that complements other existing platforms for spatial lipidomics.

References

- [1] Schnaar RL, Sandhoff R, Tiemeyer M, et al. Glycosphingolipids. In: Varki A, Cummings RD, Esko JD, et al., editors. *Essentials of Glycobiology* [Internet]. 4th edition. Cold Spring Harbor (NY): Cold Spring Harbor Laboratory Press; 2022. Chapter 11. Available from: <https://www.ncbi.nlm.nih.gov/books/NBK579905/>
- [2] D'Angelo G, Capasso S, Sticco L, Russo D (2013). *Glycosphingolipids: Synthesis and Functions*. *Febs J*, **280**(24), 6338–6353.
- [3] Zhang T, Waard AA de, Wuhrer M, Spaapen RM (2019). *The Role of Glycosphingolipids in Immune Cell Functions*. *Front Immunol*, **10**, 90.
- [4] Bien T, Perl M, Machmüller AC, Nitsche U, Conrad A, Johannes L, Müthing J, Soltwisch J, Janssen K-P, Dreisewerd K (2020). *MALDI-2 Mass Spectrometry and Immunohistochemistry Imaging of Gb3Cer, Gb4Cer, and Further Glycosphingolipids in Human Colorectal Cancer Tissue*. *Anal Chem*, **92**(10), 7096–7105.
- [5] Wallom K-L, Fernández-Suárez ME, Priestman DA, Vruchte D te, Huebecker M, Hallett PJ, Isacson O, Platt FM (2022). *Glycosphingolipid Metabolism and Its Role in Ageing and Parkinson's Disease*. *Glycoconjugate J*, **39**(1), 39–53.
- [6] Wong M, Xu G, Park D, Barboza M, Lebrilla CB (2018). *Intact Glycosphingolipidomic Analysis of the Cell Membrane during Differentiation Yields Extensive Glycan and Lipid Changes*. *Sci Rep*, **8**(1), 10993.
- [7] Rossdam C, Konze SA, Oberbeck A, Rapp E, Gerardy-Schahn R, Itzstein M von, Buettner FFR (2019). *Approach for Profiling of Glycosphingolipid Glycosylation by Multiplexed Capillary Gel Electrophoresis Coupled to Laser-Induced Fluorescence Detection To Identify Cell-Surface Markers of Human Pluripotent Stem Cells and Derived Cardiomyocytes*. *Anal Chem*, **91**(10), 6413–6418.
- [8] Wang D, Madunić K, Zhang T, Mayboroda OA, Lageveen-Kammeijer GSM, Wuhrer M (2022). *High Diversity of Glycosphingolipid Glycans of Colorectal Cancer Cell Lines Reflects the Cellular Differentiation Phenotype*. *Mol Cell Proteomics*, **21**(6), 100239.
- [9] Colsch B, Woods AS (2010). *Localization and Imaging of Sialylated Glycosphingolipids in Brain Tissue Sections by MALDI Mass Spectrometry*. *Glycobiology*, **20**(6), 661–667.
- [10] Zhang Y, Wang B, Jin W, Wen Y, Nan L, Yang M, Liu R, Zhu Y, Wang C, Huang L, Song X, Wang Z (2019). *Sensitive and Robust MALDI-TOF-MS Glycomics Analysis Enabled by Girard's Reagent T on-Target Derivatization (GTOD) of Reducing Glycans*. *Anal Chim Acta*, **1048**, 105–114.
- [11] Bednařík A, Bölsker S, Soltwisch J, Dreisewerd K (2018). *An On-Tissue Paternò-Büchi Reaction for Localization of Carbon–Carbon Double Bonds in Phospholipids and Glycolipids by Matrix-Assisted Laser-Desorption–Ionization Mass-Spectrometry Imaging*. *Angew Chem*, **130**(37), 12268–12272.
- [12] Vens-Cappell S, Kouzel IU, Kettling H, Soltwisch J, Bauwens A, Porubsky S, Müthing J, Dreisewerd K (2016). *On-Tissue Phospholipase C Digestion for Enhanced MALDI-MS Imaging of Neutral Glycosphingolipids*. *Anal Chem*, **88**(11), 5595–5599.
- [13] Thomas MJ, Collinge E, Witt M, Lozano DCP, Vane CH, Moss-Hayes V, Barrow MP (2019). *Petroleomic Depth Profiling of Staten Island Salt Marsh Soil: 2w Detection FTICR MS Offers a New Solution for the Analysis of Environmental Contaminants*. *Sci Total Environ*, **662**, 852–862.
- [14] Yang E, Dufresne M, Chaurand P (2019). *Enhancing Ganglioside Species Detection for MALDI-TOF Imaging Mass Spectrometry in Negative Reflectron Mode*. *Int J Mass Spectrom*, **437**, 3–9.
- [15] Strohal M, Hassman M, Kosata B, Kodicek M (2008). *mMass Data Miner: An Open Source Alternative for Mass Spectrometric Data Analysis*. *Rapid Comm Mass Spectrom*, **22**(6), 905–908.
- [16] Muralidharan S, Shimobayashi M, Ji S, Burla B, Hall MN, Wenk MR, Torta F (2021). *A Reference Map of Sphingolipids in Murine Tissues*. *Cell Reports*, **35**(11), 109250.
- [17] Sipione S, Monyror J, Galleguillos D, Steinberg N, Kadam V (2020). *Gangliosides in the Brain: Physiology, Pathophysiology and Therapeutic Applications*. *Front Neurosci*, **14**, 572965.
- [18] Palmer A, Phapale P, Chernyavsky I, Lavigne R, Fay D, Tarasov A, Kovalev V, Fuchser J, Nikolenko S, Pineau C, Becker M, Alexandrov T (2016). *FDR-Controlled Metabolite Annotation for High-Resolution Imaging Mass Spectrometry*. *Nat Methods*, **14**(1), 57–60.
- [19] Alexandrov T, Ovchinnikova K, Palmer A, Kovalev V, Tarasov A, Stuart L, Nigmatzianov R, Fay D, Contributors KM, Gaudin M, Lopez CG, Vetter M, Swales J, Bokhart M, Kompauer M, McKenzie J, Rappez L, Velickovic D, Lavigne R, Zhang G, Thinagaran D, Ruhland E, Sans M, Triana S, Sammour DA, Aboulmagd S, Bagger C, Strittmatter N, Rigopoulos A, Gemperline E, Joensen AM, Geier B, Quiason C, Weaver E, Prasad M, Balluff B, Nagornov K, Li L, Linscheid M, Hopf C, Heintz D, Liebeke M, Spengler B, Boughton B, Janfelt C, Sharma K, Pineau C, Anderton C, Ellis S, Becker M, Pánczél J, Violante GD, Muddiman D, Goodwin R, Eberlin L, Takats Z, Shahidi-Latham S (2019). *METASPACE: A Community-Populated Knowledge Base of Spatial Metabolomes in Health and Disease*. *Biorxiv*, 539478.

For Research Use Only. Not for use in clinical diagnostic procedures.

Bruker Switzerland AG

Fällanden · Switzerland
Phone +41 44 825 91 11

Bruker Scientific LLC

Billerica, MA · USA
Phone +1 (978) 663-3660



ms.sales.bdal@bruker.com – www.bruker.com

Learn more at www.bruker.com/solarix